AIP Advances

Thermal dynamics of thermoelectric phenomena from frequency resolved methods

J. García-Cañadas and G. Min

Citation: AIP Advances **6**, 035008 (2016); doi: 10.1063/1.4943958
View online: http://dx.doi.org/10.1063/1.4943958
View Table of Contents: http://scitation.aip.org/content/aip/journal/adva/6/3?ver=pdfcov
Published by the AIP Publishing

Articles you may be interested in

A Method for testing the integrated thermal resistance of thermoelectric modules
Rev. Sci. Instrum. **84**, 114903 (2013); 10.1063/1.4828339

Time and frequency resolved dynamics of Ar Br 2
J. Chem. Phys. **127**, 164309 (2007); 10.1063/1.2794332

Scattering methods applied to lattice dynamics in thermoelectric materials
J. Acoust. Soc. Am. **121**, 3090 (2007); 10.1121/1.4781956

Methods for surface roughness elimination from thermal-wave frequency scans in thermally inhomogeneous solids
J. Appl. Phys. **90**, 1255 (2001); 10.1063/1.1383579

Thermal conductivity, thermoelectric power, and thermal diffusivity from the same apparatus
Am. J. Phys. **52**, 569 (1984); 10.1119/1.13604

Reuse of AIP Publishing content is subject to the terms at: https://publishing.aip.org/authors/rights-and-permissions. IP: 131.251.254.248 On: Mon, 14 Mar 2016 09:57:08

Thermal dynamics of thermoelectric phenomena from frequency resolved methods

J. García-Cañadas[a] and G. Min
School of Engineering, Cardiff University, Cardiff, CF24 3AA, United Kingdom

(Received 31 July 2015; accepted 29 February 2016; published online 9 March 2016)

Understanding the dynamics of thermoelectric (TE) phenomena is important for the detailed knowledge of the operation of TE materials and devices. By analyzing the impedance response of both a single TE element and a TE device under suspended conditions, we provide new insights into the thermal dynamics of these systems. The analysis is performed employing parameters such as the thermal penetration depth, the characteristic thermal diffusion frequency and the thermal diffusion time. It is shown that in both systems the dynamics of the thermoelectric response is governed by how the Peltier heat production/absorption at the junctions evolves. In a single thermoelement, at high frequencies the thermal waves diffuse semi-infinitely from the junctions towards the half-length. When the frequency is reduced, the thermal waves can penetrate further and eventually reach the half-length where they start to cancel each other and further penetration is blocked. In the case of a TE module, semi-infinite thermal diffusion along the thickness of the ceramic layers occurs at the highest frequencies. As the frequency is decreased, heat storage in the ceramics becomes dominant and starts to compete with the diffusion of the thermal waves towards the half-length of the thermoelements. Finally, the cancellation of the waves occurs at the lowest frequencies. It is demonstrated that the analysis is able to identify and separate the different physical processes and to provide a detailed understanding of the dynamics of different thermoelectric effects. © *2016 Author(s). All article content, except where otherwise noted, is licensed under a Creative Commons Attribution (CC BY) license (http://creativecommons.org/licenses/by/4.0/).* [http://dx.doi.org/10.1063/1.4943958]

I. INTRODUCTION

Frequency resolved methods such as impedance spectroscopy has been proved very successful for the characterization of a variety of systems of great technological interest.[1–5] The potential of these methods, unlike experiments performed in the time domain, typically difficult to analyze and with responses commonly governed by overlapping processes, resides in their high sensitivity and their ability to separate the different physical processes occurring in the devices.[6] In frequency resolved methods, excitation waves can be used to restrict the response of the physical processes by manipulating the frequency of excitation. When high frequencies are employed, only quick processes can be observed. As the frequency is decreased, slower processes are allowed which start to influence the system response. The variation of the frequency can span several orders of magnitude, which provides a high sensitivity of the system dynamics.

In a thermoelectric (TE) material, different processes occur when a constant current is applied through it. First, an initial potential difference is established across the element by an external electric field which produces the current. Then, due to the Peltier effect, heat is released at one of the junctions and absorbed at the other, gradually creating a temperature difference across the element. This temperature difference separates carriers in the material which induces a Seebeck potential difference due to the Seebeck effect. This Seebeck voltage slows down the flow of the carriers

[a]Corresponding author: garciaj@uji.es Current address: Department of Industrial Systems Engineering and Design, Universitat Jaume I, Campus del Riu Sec, 12071 Castellon (Spain)

 ©Author(s) 2016.

Reuse of AIP Publishing content is subject to the terms at: https://publishing.aip.org/authors/rights-and-permissions. IP: 131.251.254.248 On: Mon, 14 Mar 2016 09:57:08

and decreases the current, increasing the system resistance. All these processes have distinct time scales and are governed by different parameters. By using impedance spectroscopy, which employs ac current excitation waves, we can extract very useful information about the dynamics of these fundamental TE processes, which provides a unique detailed knowledge of the system operation. This detailed analysis, in despite of the fact that previous work has been reported in the application of frequency resolved methods in the TE field,[7–9] has not been developed so far. Moreover, the transient behavior of thermoelectric elements and devices is less investigated in comparison to steady state phenomena and operation of devices in this regime has been claimed to enhance their performance,[10,11] therefore there is a need of fundamental studies in this field.

Our previous work[9] analyzed the impedance response in a single TE material and the case of a TE device by solving the heat equation in the frequency domain. It also provided experimental validation of the theoretical models. However, that study focused on the temperature variations at the junctions and did not analyze the complete thermal dynamics in the whole system, which can provide useful additional information. By using our previous models as a basis, we focus here on a detailed description of the evolution of the thermal waves and the internal thermal gradients in the whole system. The analysis introduces different dynamic parameters such as the thermal penetration depth and thermal diffusion times which were not previously included. In addition, the different regimes of behavior previously observed are now analyzed in detail, which allows the identification of semi-infinite diffusion and interacting regimes. Through this more extended analysis the identification and separation of the different physical processes occurring in the device is achieved, which provides a unique detailed understanding of the system dynamics.

II. EXPERIMENTAL PART

Impedance measurements were performed both in a single thermoelement and a TE module. The impedance response of a *p*-type Bi_2Te_3 element (European Thermodynamics Ltd.) with a cross-sectional area of 1.4 x 1.4 mm^2 and a length of 1.6 mm was measured similarly to a previously reported procedure.[9] A layer of Ag paint was spread on the top and bottom sides of the element. The sample was sandwiched by two short stainless steel probes with sharp tips that were connected to the input leads of the equipment. It should be noted that stainless steel material is used here instead of copper, which was employed in the previous procedure, to minimize the cold finger effect (heat conduction through the probes). A constant current of 100 mA was applied to the element before measuring the impedance in order to settle the electrical contacts.[9] A commercial TE module (European Thermodynamics Ltd.) formed by 252 thermoelements (1 mm x 1 mm x 1.5 mm) was also measured by directly contacting to the equipment leads. Both samples were suspended in air to provide adiabatic conditions. The thickness of the ceramic plates of the module is 0.8 mm.

Impedance measurements were performed at room temperature using a PGSTAT302N potentiostat equipped with a FRA32M impedance module (Metrohm Autolab B. V.) in a frequency range of 10 mHz to 100 Hz for the thermoelement and 1 mHz to 1 kHz for the TE module. A sinusoidal signal of 20 mA (rms) in amplitude was applied without dc bias (0 A dc).

III. SINGLE THERMOELEMENT

A similar initial analysis as adopted in our previous work[9] is presented here. We consider a single thermoelement of cross-sectional area A and length L contacted by very thin metallic contacts. The element is suspended under adiabatic conditions, with ideal thermal and electric contacts and at homogeneous initial temperature T_i. A sinusoidal current wave of small amplitude oscillating around 0 A is used as the excitation signal. Due to the small current amplitude and the typically high electrical conductivity of TE materials, Joule effect is neglected in our analysis. In addition, all the TE properties are assumed to be independent on temperature. Fig. 1(a) shows the different thermal processes that appear in a *p*-type thermoelement under these assumptions. It should be noted that a constant-temperature plane is present at the half-length $L_H=L/2$, where the temperature remains at its initial value at all times.

Reuse of AIP Publishing content is subject to the terms at: https://publishing.aip.org/authors/rights-and-permissions. IP: 131.251.254.248 On: Mon, 14 Mar 2016 09:57:08

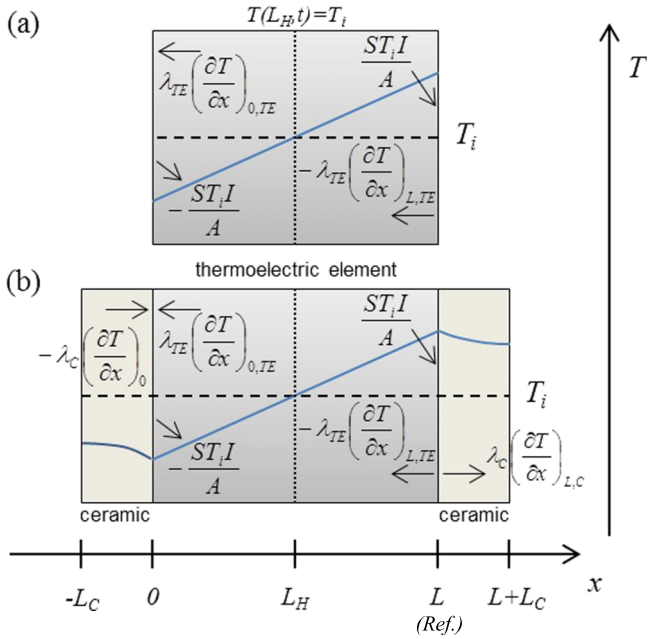

FIG. 1. Scheme of the thermal processes occurring at steady state under adiabatic conditions and constant positive current in (a) a single p-type thermoelement and (b) a thermolement sandwiched by ceramic layers. The initial homogeneous temperature (dashed line), thermal profile at steady state (solid line) and the constant temperature plane (dotted line) are represented. Arrows pointing in or out of the junctions are considered as a heat input or heat removal respectively. The reference for the potential difference is taken at $x=L$.

The heat equation of the system in Fig. 1(a) in the frequency domain is defined by,

$$\frac{\partial^2\theta}{\partial x^2} - \frac{1}{m^2}\theta = 0, \text{ at } 0 \le x \le L \tag{1}$$

where $\theta(x,j\omega)=L[T(x,t)-T_i]$ is the Laplace transform of the temperature excess respect to the initial temperature, x the position, t the time, $j=\sqrt{-1}$, ω the angular frequency and m a length defined as, $m(j\omega)=(\omega_{TE}/j\omega)^{0.5}L_H$, with $\omega_{TE}=\alpha_{TE}/L_H^2$, being α_{TE} the thermal diffusivity of the thermoelement. The boundary conditions are,

$$-\frac{ST_ii_0}{A} + \lambda_{TE}\left(\frac{\partial\theta}{\partial x}\right)_{0,TE} = 0, \text{ at } x=0 \tag{2}$$

$$\theta(L_H,j\omega) = 0, \text{ at } x=L_H \tag{3}$$

with S the Seebeck coefficient, $i_0=L[I(0,t)]$ the Laplace transform of the current I at $x=0$ and λ_{TE} the thermal conductivity of the thermoelement. It should be noted that due to the small ac amplitude of the excitation current, large changes are not expected in the temperature at the junction and $T(x=0)\approx T_i$ in the Peltier term of Eq. (2).

The solution to Eq. (1) with the above boundary conditions has the expression,

$$\theta(x,j\omega) = \frac{ST_ii_0L_H}{\lambda_{TE}A}\left(\frac{j\omega}{\omega_{TE}}\right)^{-0.5}\left\{\sinh\left[\frac{x}{L_H}\left(\frac{j\omega}{\omega_{TE}}\right)^{0.5}\right] - \cosh\left[\frac{x}{L_H}\left(\frac{j\omega}{\omega_{TE}}\right)^{0.5}\right]\tanh\left[\left(\frac{j\omega}{\omega_{TE}}\right)^{0.5}\right]\right\}. \tag{4}$$

The Seebeck potential difference $V_s=V_s(0)-V_s(L)=-S[T(0)-T(L)]$ can be obtained using $V_s=-2S[T(0)-T_i]$ due to the presence of the constant temperature plane. Hence, the ac Seebeck potential difference in the frequency domain, $-2S\theta(0,j\omega)$, can be calculated using $\theta_0=\theta(0,j\omega)=-[ST_ii_0L_H/(\lambda_{TE}A)](j\omega/\omega_{TE})^{-0.5}\tanh[(j\omega/\omega_{TE})^{0.5}]$. To determine the total potential difference, $V=V(0)-V(L)$, the ohmic voltage drop IR should be included. Then, $V=IR-2S[T(0)-T_i]$, where R accounts for the material and parasitic (contact and wires) resistances. The impedance function Z, calculated from

Reuse of AIP Publishing content is subject to the terms at: https://publishing.aip.org/authors/rights-and-permissions. IP: 131.251.254.248 On: Mon, 14 Mar 2016 09:57:08

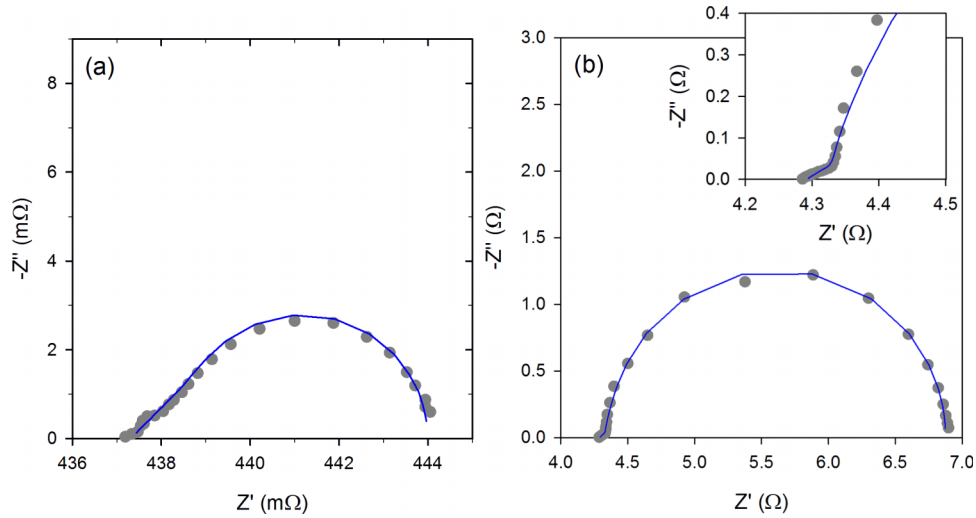

FIG. 2. Experimental impedance response (circles) of (a) a p-type Bi_2Te_3 thermoelement and (b) a commercial Bi_2Te_3-based TE module. The inset in (b) shows a magnification of the high frequency part. Lines represent the fittings to the theoretical expressions. Reprinted from J. García-Cañadas and G. Min Appl. Phys. Lett. 116, 174510 (2014). Copyright 2014 AIP Publishing LLC.

the ratio of the voltage and the current, is given by,

$$Z(j\omega) = R - \frac{2S\theta(0,j\omega)}{i_0} = R + \frac{S^2T_iL}{\lambda_{TE}A}\left(\frac{j\omega}{\omega_{TE}}\right)^{-0.5}\tanh\left[\left(\frac{j\omega}{\omega_{TE}}\right)^{0.5}\right]. \quad (5)$$

Fig. 2(a) shows the excellent agreement between the experimental response (circles) and the fit (lines) to Eq. (5). The fitting parameters obtained appear in Table I. As previously reported,[9] all the thermal properties of the element can be obtained if the S value is known (see Table I).

If we pay attention to the system dynamics, it can be observed that the terms which depend on ω, which contain the dynamic information, come from the temperature excess function θ. Fig. 3(a) shows the simulation of the impedance response of Eq. (5) (solid line) for a thermoelement with typical TE properties of Bi_2Te_3. Both n and p-type provide the same response, since S is squared in the expression. The last term of Eq. (5) is called the constant-temperature Warburg impedance,[9,12] Z_{WCT}, and clearly shows two different regimes of behavior separated around the characteristic angular frequency $\omega_d=2\pi\omega_{TE}$. A slope of 1 response (dashed line), given by $Z=R+R_{TE}(j\omega/\omega_{TE})^{-0.5}$, is observed at $\omega>>\omega_d$, being $R_{TE}=S^2T_iL/(\lambda_{TE}A)$ a TE resistance.[13] These high angular frequencies are usually lower than 600 Hz which it is when the temperature variation at the junctions starts to be established. At $\omega<<\omega_d$ the impedance response turns into a semicircle with the expression (assuming $R=0$), $Z^{-1}=1/R_{TE}+j\omega/(3C_{TE})$, where $C_{TE}=1/(R_{TE}\omega_{TE})$ is a TE capacitance.[13]

Differently from our previous work,[9] we analyze now in detail the physical meaning of these different regimes. The slope of 1 response at $\omega>>\omega_d$ represents a semi-infinite diffusion regime,[14] which can be deduced by solving the same heat equation above with the boundary condition of Eq. (3) replaced by the boundary condition of a semi-infinite system ($L\to\infty$), which takes the form

TABLE I. Fitting parameters and calculated properties from the experimental impedance measurements of Fig. 2 corresponding to a single thermoelement and a commercial TE module. The thermal properties of the element were calculated using a Seebeck coefficient value (195 μV/K) measured by a hot-probe apparatus. In brackets are typical values for Bi_2Te_3 obtained from manufacturers.

Sample	R_Ω (Ω)	R_{TE} (Ω)	ω_{TE} (rad/s)	λ_{TE} (W/m K)	α_{TE} (cm^2/s)	$C_{p,TE}$ (J/gK)	S ($\mu V/K$)	R_c (Ω)	ω_c (rad/s)
Element	0.437	0.00668	1.78	1.37 (1.50)	0.0036 (0.0037)	0.45 (0.54)	-	-	-
Module	4.292	2.585	0.24	1.62	0.0013	1.65	193.5 (200)	0.149	6.08

Reuse of AIP Publishing content is subject to the terms at: https://publishing.aip.org/authors/rights-and-permissions. IP: 131.251.254.248 On: Mon, 14 Mar 2016 09:57:08

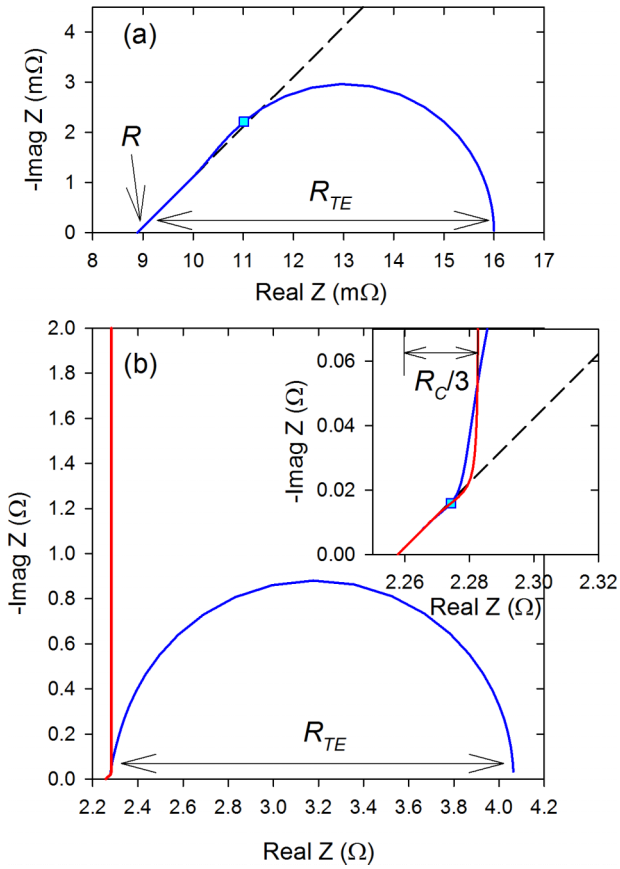

FIG. 3. Simulations of the impedance response of (a) a thermoelement and (b) a thermoelectric device. The inset in (b) is the magnification at high frequencies. The parameters employed in (a) are S=200 μV/K, λ_{TE}=1.5 W/m K, α_{TE}=3.66x10^{-3} cm^2/s, L=2 mm, A=1.5 x 1.5 mm^2, R=8.9 mΩ and ω_{TE}=0.37 rad/s. For the thermoelectric module (b) the same thermoelectric properties have been used with the addition of N=127 couples, L_C=1 mm, λ_C=36 W/m K, α_C=0.12x10^{-3} cm^2/s and ω_C=11.85 rad/s. R now takes the value R=2.26 Ω. The response at the angular frequencies ω_d and ω_{dC} are indicated by a square in (a) and (b) respectively. The dashed line represents the response of the semi-infinite regimes and the red line the impedance of a Warburg adiabatic element in series with R.

$\theta(\infty, j\omega)$=0. The solution with this new boundary condition is,

$$\theta(x, j\omega) = \frac{ST_i i_0 L_H}{\lambda_{TE} A}\left(\frac{j\omega}{\omega_{TE}}\right)^{-0.5}\left\{\sinh\left[\frac{x}{L_H}\left(\frac{j\omega}{\omega_{TE}}\right)^{0.5}\right] - \cosh\left[\frac{x}{L_H}\left(\frac{j\omega}{\omega_{TE}}\right)^{0.5}\right]\right\}, \qquad (6)$$

which at x=0 is $\theta(0)$=-[$ST_i i_0 L_H/(\lambda_{TE}A)$]$(j\omega/\omega_{TE})^{-0.5}$ and clearly agrees with the slope of 1 regime of the impedance, Z=R+$R_{TE}(j\omega/\omega_{TE})^{-0.5}$. Hence, under this regime, the two thermal waves produced by the heat production and the heat absorption induced by the Peltier effect at the junctions, diffuse "freely" inside the thermoelement, i. e., without noticing the influence of each other. The waves do not have enough time to penetrate and reach the half-length of the thermoelement. The boundary condition at x=L_H has no effect in this case. We would like to emphasize that as described by the thermal diffusivity α_{TE}=$\lambda_{TE}/(\rho C_p)$, diffusion involves both the storage of heat (absorption or release), governed by the product of the mass density ρ and the specific heat C_p, and the heat conduction, governed by λ_{TE} and the temperature gradient.

Eq. (4) can be expressed as $\theta(x, j\omega)$= – θ_0\{sinh[-$(x/L_H)(j\omega/\omega_{TE})^{0.5}$]/tanh[$(j\omega/\omega_{TE})^{0.5}$]-cosh[-$(x/L_H)(j\omega/\omega_{TE})^{0.5}$]\}and it is represented in Fig. 4(a) for 3 different angular frequencies. It can be observed that the maximum amplitudes always occur at the junctions and decay with penetration towards L_H. The amplitude of the thermal wave of angular frequency ω_d (black solid line) is reduced to 1 % of the amplitude at the junction (θ=0.01θ_0) at $x \approx L_H$ and it can be considered

Reuse of AIP Publishing content is subject to the terms at: https://publishing.aip.org/authors/rights-and-permissions. IP: 131.251.254.248 On: Mon, 14 Mar 2016 09:57:08

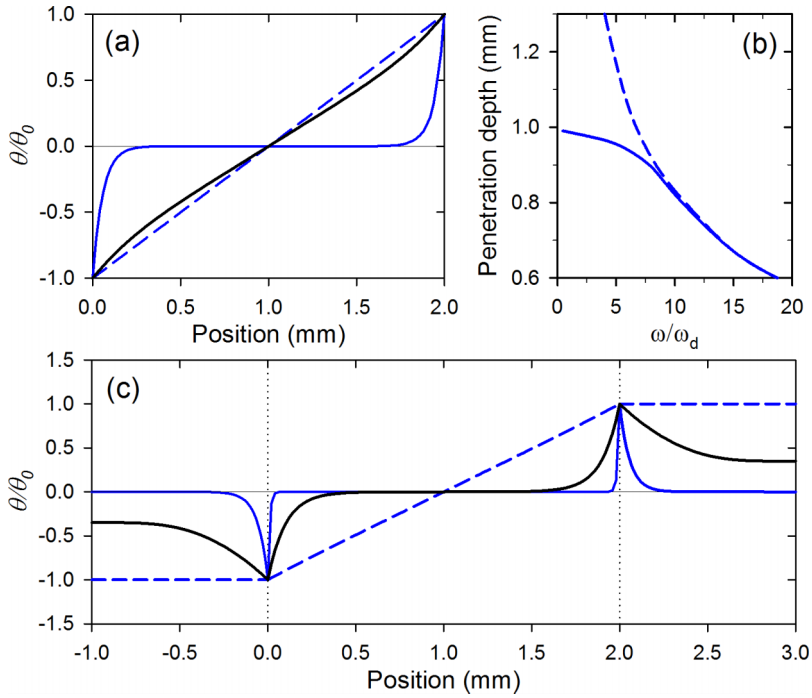

FIG. 4. (a) Magnitude of the ac thermal waves normalized respect to the magnitude at x=0 as a function of position for a 2 mm long single thermoelement at ω=100ω_d (blue solid line), ω=ω_d (black solid line) and ω=0.01ω_d (dashed line). (b) Penetration depth respect to the angular frequency normalized to ω_d for the semi-infinite (dashed line) and actual (solid line) models in the single thermoelement. (c) Same as (a) for the thermoelement sandwiched by ceramic layers at ω=100ω_{dC} (blue solid line), ω=ω_{dC} (black solid line) and ω=0.01ω_{dC} (dashed line). The magnitudes in (a) and (c) have been made negative at x<1 mm to better match the real temperature profiles.

that the wave can penetrate up to L_H. More generally, the position at which the amplitude of a thermal wave of certain angular frequency is reduced to 1 % is given by m_d=4.6m$\sqrt{2}$ (dashed line in Fig 3(b)),[15] which we consider as the thermal penetration depth. It should be noted that m_d only provides a correct penetration depth value when ω>>ω_d. Using m_d it can be considered that the system behaves semi-infinitely at m_d<<L_H, which is equivalent to ω>>ω_d, as observed in Fig. 3(b). On the other hand, the period corresponding to ω_d can be defined as the thermal diffusion time τ_d=L_H^2/α_{TE}, which can be considered as the time required by the thermal wave to travel from the junction to the half-length.

At ω<<ω_d (or m_d>>L_H) the thermal waves have enough time to penetrate up to L_H and the impedance response is governed by their interaction. At half-length the heat input from the right side equals the heat extraction from the left and the thermal waves cannot penetrate further, progressively reaching the dc regime (Fig. 4(a), dashed line). We would like to remark that the existence of thermal waves has been experimentally confirmed previously by Downey et al. by infrared imaging.[7]

IV. TE DEVICE

In the classical structure of a TE module, the thermoelements are connected electrically in series by metallic strips and sandwiched between two ceramic layers of thickness L_C. A similar initial description as in our previous work[9] is again adopted. We consider a reduced one dimensional model for a TE device formed by 2N basic units thermally in parallel, where N is the number of thermocouples. One of the basic units is shown in Fig. 1(b). All thermoelements are considered to have the same TE properties and the absolute value |S| is used. The influence of the metallic connectors will be neglected due to their short thickness and high thermal conductivity. The thermal

Reuse of AIP Publishing content is subject to the terms at: https://publishing.aip.org/authors/rights-and-permissions. IP: 131.251.254.248 On: Mon, 14 Mar 2016 09:57:08

spreading/constriction occurring at the junctions[16] will be also neglected for simplicity. The presence of the ceramics in a TE device makes the Peltier heat generated at each junction to be able to diffuse along their thickness (Fig. 1(b)) apart from the diffusion towards the half-length of the thermoelements. This will significantly influence the impedance response.

The heat diffusion equation in the ceramic layer,

$$\frac{\partial^2\theta}{\partial x^2} - \frac{1}{m_C^2}\theta = 0, \text{ at } -L_C \leq x \leq 0 \tag{7}$$

where, $m_C=(j\omega/\omega_C)^{0.5}L_C$, $\omega_C=\alpha_C/L_C^2$ and α_C is the thermal diffusivity of the ceramic. Eq. (7) has to be solved in addition to Eq. (1) for the thermoelement with new boundary conditions,

$$\left(\frac{\partial\theta}{\partial x}\right)_{-L_C,C} = 0, \tag{8}$$

$$-\frac{ST_i i_0}{A} - \lambda_C\left(\frac{\partial\theta}{\partial x}\right)_{0,C} + \lambda_{TE}\left(\frac{\partial\theta}{\partial x}\right)_{0,TE} = 0, \text{ at } x=0 \tag{9}$$

$$\theta(L_H, j\omega) = 0, \tag{10}$$

$$\theta(0, j\omega)_C = \theta(0, j\omega)_{TE}, \tag{11}$$

where, λ_C is the thermal conductivity of the ceramic. After solving the corresponding systems of equations, the solutions of the heat equations for the ceramic and the thermoelement have the expressions,

$$\theta(x, j\omega) = -\frac{ST_i i_0}{A}\frac{\tanh\left[\left(\frac{j\omega}{\omega_C}\right)^{0.5}\right]\sinh\left[\frac{x}{L_C}\left(\frac{j\omega}{\omega_C}\right)^{0.5}\right] + \cosh\left[\frac{x}{L_C}\left(\frac{j\omega}{\omega_C}\right)^{0.5}\right]}{\left\{\frac{L_C}{\lambda_C}\left(\frac{j\omega}{\omega_C}\right)^{-0.5}\coth\left[\left(\frac{j\omega}{\omega_C}\right)^{0.5}\right]\right\}^{-1} + \left\{\frac{L_H}{\lambda_{TE}}\left(\frac{j\omega}{\omega_{TE}}\right)^{-0.5}\tanh\left[\left(\frac{j\omega}{\omega_{TE}}\right)^{0.5}\right]\right\}^{-1}},$$
$$\text{at } -L_C \leq x \leq 0 \tag{12}$$

$$\theta(x, j\omega) = \frac{ST_i i_0}{A}\frac{\coth\left[\left(\frac{j\omega}{\omega_{TE}}\right)^{0.5}\right]\sinh\left[\frac{x}{L_H}\left(\frac{j\omega}{\omega_{TE}}\right)^{0.5}\right] - \cosh\left[\frac{x}{L_H}\left(\frac{j\omega}{\omega_H}\right)^{0.5}\right]}{\left\{\frac{L_C}{\lambda_C}\left(\frac{j\omega}{\omega_C}\right)^{-0.5}\coth\left[\left(\frac{j\omega}{\omega_C}\right)^{0.5}\right]\right\}^{-1} + \left\{\frac{L_H}{\lambda_{TE}}\left(\frac{j\omega}{\omega_{TE}}\right)^{-0.5}\tanh\left[\left(\frac{j\omega}{\omega_{TE}}\right)^{0.5}\right]\right\}^{-1}},$$
$$\text{at } 0 \leq x \leq L. \tag{13}$$

At $x=0$, both expressions become equal and take the form,

$$\theta(0, j\omega) = -\frac{ST_i i_0}{A}\left\{\left\{\frac{L_C}{\lambda_C}\left(\frac{j\omega}{\omega_C}\right)^{-0.5}\coth\left[\left(\frac{j\omega}{\omega_C}\right)^{0.5}\right]\right\}^{-1} + \left\{\frac{L_H}{\lambda_{TE}}\left(\frac{j\omega}{\omega_{TE}}\right)^{-0.5}\tanh\left[\left(\frac{j\omega}{\omega_{TE}}\right)^{0.5}\right]\right\}^{-1}\right\}^{-1}. \tag{14}$$

In the case of the TE device, the total potential difference is $V=IR-4N|S|[T(0)-T_i]$, which leads to the impedance function for the TE module,

$$Z(j\omega) = R + 4N\frac{S^2T_i}{A}\left\{\left\{\frac{L_C}{\lambda_C}\left(\frac{j\omega}{\omega_C}\right)^{-0.5}\coth\left[\left(\frac{j\omega}{\omega_C}\right)^{0.5}\right]\right\}^{-1} + \left\{\frac{L_H}{\lambda_{TE}}\left(\frac{j\omega}{\omega_{TE}}\right)^{-0.5}\tanh\left[\left(\frac{j\omega}{\omega_{TE}}\right)^{0.5}\right]\right\}^{-1}\right\}^{-1}$$
$$= R + \frac{1}{Z_{Wa}^{-1} + Z_{WCT}^{-1}}, \tag{15}$$

being $Z_{Wa}=R_C(j\omega/\omega_C)^{-0.5}\coth[(j\omega/\omega_C)^{0.5}]$ the impedance of an adiabatic Warburg element,[9,12] with $R_C=4NS^2T_iL_C/(\lambda_C A)$ being the TE resistance induced by the ceramic layer, and $Z_{WCT}=R_{TE}(j\omega/\omega_{TE})^{-0.5}\tanh[(j\omega/\omega_{TE})^{0.5}]$, where now $R_{TE}=2NS^2T_iL/(\lambda_{TE}A)$ takes into account all the thermoelements of the TE device.

Fig. 2(b) shows the good correlation between the experimental impedance measurements (circles) of a commercial TE module and the fit (lines) to Eq. (15). The fitting parameters and all the TE

Reuse of AIP Publishing content is subject to the terms at: https://publishing.aip.org/authors/rights-and-permissions. IP: 131.251.254.248 On: Mon, 14 Mar 2016 09:57:08

properties (Table I) of the module, can be calculated in this case using the thermal conductivity of the ceramic material without the need to independently measure S.[9]

Differently from our previous work,[9] we focus now on extracting the physical meaning of the processes which govern the impedance response. Fig. 3(b) (blue solid line) shows the impedance response of Eq. (15). It can be seen that under the assumption that $\lambda_C >> \lambda_{TE}$, the impedance response of Eq. (15) becomes $Z=R+Z_{Wa}$ (red line in Fig. 3(b)) and is only governed by the thermal properties of the ceramic. In this case, two different regimes separated by the characteristic frequency $\omega_{dC} = 2\pi\omega_C$ can be clearly identified. A slope of 1 trend occurs at $\omega >> \omega_{dC}$, given by $Z = R+R_C(j\omega/\omega_C)^{-0.5}$ (dashed line in Fig. 3(b)), which corresponds to the semi-infinite thermal diffusion of the thermal waves originated at the junctions towards the outer edges of the ceramics. On the other hand, a vertical line develops at $\omega << \omega_{dC}$, where $Z=R+R_C/3+C_C/(j\omega)$, being $C_C=R_C\omega_C$ a TE capacitance induced by the ceramics.

The same features of the semi-infinite regime identified in the case of the single thermoelement can be adopted here. A profile of the amplitude of the thermal waves in this regime is represented in Fig. 4(c) (blue solid line). It can be observed that the diffusion of the thermal waves towards the ceramic outer edges occurs much more significantly than towards the half-length of the thermoelement. In this regime the thermal penetration depth can be defined as $m_{dC}=4.6m_C\sqrt{2}$, being $m_C = (\omega_C/j\omega)^{0.5}L_C$. At $\omega << \omega_{dC}$ (or $m_{dC} >> L_C$), the waves starts noticing the adiabatic boundary condition and the thermal wave cannot travel further, the change in the temperature of the ceramics becomes more significant and thus the impedance response becomes mainly governed by the heat storage, producing the vertical line of Fig. 3(b) (red line). A thermal diffusion time corresponding to the period of the wave of angular frequency ω_{dC} can be defined as $\tau_{dC}=L_C^2/\alpha_C$, which can be estimated as the time required by the thermal wave originated at the junction, to cover the distance L_C.

When the complete impedance response of Eq. (15) is represented (Fig. 3(b), blue solid line), it can be observed that the vertical trend is hardly noticed and the response turns into a large semicircle. This occurs since the differences between λ_C and λ_{TE} are not very large and a competition of the heat storage process in the ceramics with the diffusion of the thermal waves towards the half-length of the thermoelement occurs (Fig. 4(c), blue solid line). At the lowest frequencies the thermal waves can reach L_H and start to interact producing the closing of the semicircle and the linear thermal profiles of Fig. 4(c) (dashed line).

V. CONCLUSIONS

The thermal dynamics of both a single TE element and a TE device has been analyzed by impedance spectroscopy. The analysis allows the identification of the different processes governing the system response which define the different regimes in the impedance spectra. From the analysis dynamic parameters such as the thermal penetration depth and the thermal diffusion time have been introduced. These parameters define the dynamic processes which are governed in both systems by the evolution of the Peltier heat originated at the junctions.

In the case of a single thermoelement, the thermal waves penetrate towards the half-length of the thermoelement semi-infinitely at high frequencies. At lower frequencies both waves reach the half-length and start to interact, cancelling each other and avoiding their further penetration.

In a TE device, due to the higher thermal conductivity of the ceramic layers, the thermal waves initially diffuse predominantly towards the outer edges at high frequencies. At mid frequencies, they have enough time to cover the ceramic thickness and the heat is predominantly stored in the ceramics. Consequently, heat storage occurs simultaneously to the thermal diffusion towards the half-length of the thermoelements. At the lowest frequencies, the thermal waves penetrate up to the half-length and start cancelling each other until the dc regime is reached.

This analysis demonstrates the possibility of identifying the different physical processes occurring at distinct time scales and provides a detailed understanding of the dynamics of TE phenomena, which can lead to new strategies in the characterization and development of materials and devices, such as their transient operation.[10,11] Moreover, it also offers the possibility to extend the study to more realistic operating conditions, which are not typically analyzed in the literature.

Reuse of AIP Publishing content is subject to the terms at: https://publishing.aip.org/authors/rights-and-permissions. IP: 131.251.254.248 On: Mon, 14 Mar 2016 09:57:08

ACKNOWLEDGMENTS

The authors wish to acknowledge financial support from the Accelerated Metallurgy Project, which was co-funded by the European Commission in the 7th Framework Programme (Contract No. NMP4-LA-2011-263206), by the European Space Agency and by the individual partner organizations.

[1] F. Fabregat-Santiago, G. Garcia-Belmonte, I. Mora-Sero, and J. Bisquert, Phys. Chem. Chem. Phys. **13**, 9083 (2011).
[2] I. Mora-Sero, G.A. Garcia-Belmonte, P.P. Boix, M.A. Vazquez, and J. Bisquert, Energy Environ. Sci. **2**, 678 (2009).
[3] X.Z. Yuan, H.J. Wang, J.C. Sun, and J.J. Zhang, Int. J. Hydrogen Energy **32**, 4365 (2007).
[4] R. Kotz, M. Hahn, and R. Gallay, J. Power Sources **154**, 550 (2006).
[5] G.W. Walter, Corros. Sci. **26**, 681 (1986).
[6] J. Bisquert and F. Fabregat-Santiago, "Chapter 12 Impedance Spectroscopy: A general Introduction and Application to Dye-sensitized Solar cells," in *Dye-Sensitized Solar Cells*, edited by K. Kalyanasundaram (EPFL Press, 2010), p. 457.
[7] A.D. Downey, T.P. Hogan, and B. Cook, Rev. Sci. Instrum. **78**, 93904 (2007).
[8] A. De Marchi and V. Giaretto, Rev. Sci. Instrum. **82**, 104904 (2011).
[9] J. García-Cañadas and G. Min, J. Appl. Phys. **116**, 174510 (2014).
[10] J.G. Stockholm, C. Goupil, P. Maussion, and H. Ouerdane, J. Electron. Mater. **44**, 1768 (2014).
[11] H. Zhou, J. Thingna, P. Hänggi, J.-S. Wang, and B. Li, Sci. Rep. **5**, 14870 (2015).
[12] E. Warburg, Ann. Phys. **311**, 125 (1901).
[13] J. García-Cañadas and G. Min, J. Electron. Mater. **43**, 2411 (2014).
[14] J.J. Martínez-Flores, L. Licea-Jiménez, S.A. Pérez García, J. Rodríguez-Viejo, and J. Alvarez-Quintana, J. Appl. Phys. **112**, 94901 (2012).
[15] M. Jakob, *Heat Transfer, Volume 1* (John Wiley & Sons, New York, 1949).
[16] F. Casalegno, A. De Marchi, and V. Giaretto, Rev. Sci. Instrum. **84**, 024901 (2013).

Reuse of AIP Publishing content is subject to the terms at: https://publishing.aip.org/authors/rights-and-permissions. IP: 131.251.254.248 On: Mon, 14 Mar 2016 09:57:08